A Synthetic Spring-Neap Tidal Cycle for Long-Term Morphodynamic Models

Schrijvershof, R. A.; van Maren, D. S.; Torfs, P. J. J. F.; Hoitink, A. J. F.

DOI
10.1029/2022JF006799

Publication date
2023

Document Version
Final published version

Published in
Journal of Geophysical Research: Earth Surface

Citation (APA)
Schrijvershof, R. A., van Maren, D. S., Torfs, P. J. J. F., & Hoitink, A. J. F. (2023). A Synthetic Spring-Neap Tidal Cycle for Long-Term Morphodynamic Models. *Journal of Geophysical Research: Earth Surface*, *128*(3), Article e2022JF006799. https://doi.org/10.1029/2022JF006799

JGR Earth Surface

RESEARCH ARTICLE
10.1029/2022JF006799

Special Section:
Prediction in coastal geomorphology

A Synthetic Spring-Neap Tidal Cycle for Long-Term Morphodynamic Models

R. A. Schrijvershof[1,2], D. S. van Maren[2,3,4], P. J. J. F. Torfs[1], and A. J. F. Hoitink[1]

[1]Environmental Sciences Group, Wageningen University & Research, Wageningen, The Netherlands, [2]Deltares, Delft, The Netherlands, [3]State Key Lab of Estuarine and Coastal Research, East China Normal University, Shanghai, China, [4]Faculty of Civil Engineering and Geosciences, Delft University of Technology, Delft, The Netherlands

Key Points:

- A new approach to devise periodic tidal boundary conditions for long-term morphodynamic simulations is developed
- The new method better represents tidal water level dynamics, bed shear stress, and residual sand transport
- Including spring-neap variations in the tidal input reduction approach particularly improves hydrodynamics in intertidal areas

Correspondence to:

R. A. Schrijvershof,
reinier.schrijvershof@wur.nl;
reinier.schrijvershof@deltares.nl

Citation:

Schrijvershof, R. A., van Maren, D. S., Torfs, P. J. J. F., & Hoitink, A. J. F. (2023). A synthetic spring-neap tidal cycle for long-term morphodynamic models. *Journal of Geophysical Research: Earth Surface*, *128*, e2022JF006799. https://doi.org/10.1029/2022JF006799

Received 15 JUN 2022
Accepted 16 FEB 2023

Author Contributions:

Conceptualization: R. A. Schrijvershof, D. S. van Maren, P. J. J. F. Torfs, A. J. F. Hoitink
Data curation: R. A. Schrijvershof
Formal analysis: R. A. Schrijvershof
Funding acquisition: A. J. F. Hoitink
Investigation: R. A. Schrijvershof
Methodology: R. A. Schrijvershof, D. S. van Maren, P. J. J. F. Torfs, A. J. F. Hoitink
Project Administration: R. A. Schrijvershof, A. J. F. Hoitink
Resources: R. A. Schrijvershof
Software: R. A. Schrijvershof

Abstract Existing tidal input reduction approaches applied in accelerated morphodynamic simulations aim to capture the dominant tidal forces in a single or double representative tidal cycle, often referred to as a "morphological tide." These strongly simplified tidal signals fail to represent the tidal extremes and hence poorly allow to represent hydrodynamics in the intertidal areas. Here, a generic method is developed to construct a synthetic spring-neap tidal cycle that (a) represents the original signal; (b) is exactly periodic; and (c) is derived directly from tidal time series or harmonic constituents. The starting point is a fortnightly modulation of the semidiurnal tide to represent spring-neap variations, while conserving periodicity. Diurnal tides and higher harmonics of the semidiurnal tide are included to represent the asymmetry of the tide. The amplitudes and phases of the synthetic signal are then fitted to histograms of water levels and water level gradients derived from the original sea surface elevation time series. A depth-averaged model of the Ems estuary (The Netherlands) demonstrates the effects of alternative tidal input reduction techniques. Adopting the new approach, the along-estuary variation in tidal wave shape is well-represented, leading to an improved representation of extreme tidal conditions. Especially the more realistic representation of intertidal dynamics improves the overall hydrodynamics and residual sand transport patterns, approaching nonschematized tidal dynamics.

Plain Language Summary The daily emerging and inundation of tidal flats occurs much faster than the emerging or drowning of tidal flats by sedimentation or erosion (hours vs. years, respectively). To efficiently simulate years of erosion and deposition, an acceleration factor is applied to models that simulate the long-term bed level developments. Tidal information used to force these models requires an input reduction technique that copes with the fact that successive spring-neap cycles are never identical. In this paper, a tidal input reduction method is developed that yields a synthetic, periodic tidal signal representing the amplitude and asymmetry variation present in a multiyear tidal signal. These variations are not captured well in existing, more limited, approaches for tidal input reduction, likely restricting their application for longer timescales, because neglecting these variations can cause errors to accumulate in the course of a simulation. Results from a numerical model forced with the synthetic signal shows that, compared to existing approaches, particularly the intertidal dynamics and residual sand transports better represent the multiscale tidal conditions. Therefore, the new tidal input reduction method should improve the channel-shoal exchange in long-term estuarine models, presumably allowing for a more realistic assessment of erosion and deposition in these areas.

1. Introduction

The long-term or multidecadal evolution of estuaries and tidal basins is largely controlled by the interaction between hydrodynamic forcing and the sediment bed (De Swart & Zimmerman, 2009). This morphodynamic dependence on hydrodynamics allows for a quantitative investigation of the evolution of tidal environments using process-based numerical models. Contemporary studies often address the increasing impacts of anthropogenic activities (Syvitski et al., 2009) jeopardizing ecosystem services and potentially leading to morphological instability (Hoitink et al., 2020). Although numerical bed evolution models were originally developed to predict the short-term morphological response to engineering measures (De Vriend et al., 1993), their predictive skill appears to improve when the timescales related to the investigated changes (T_c) and the timescale at which the model attains dynamic equilibrium (T_e) are longer (Dam et al., 2016). The developments from the initial conditions toward the model's dynamic equilibrium may obscure the morphodynamic impact of the interventions where the model was originally designed for. As a consequence, process-based models are increasingly used

Supervision: D. S. van Maren, A. J. F. Hoitink
Validation: R. A. Schrijvershof
Visualization: R. A. Schrijvershof
Writing – original draft: R. A. Schrijvershof

to investigate not only decadal but also centennial and even millennial morphological evolution of estuarine and tidal environments (e.g., Braat et al., 2017; Dastgheib et al., 2008; Nnafie et al., 2018; Van der Wegen & Roelvink, 2012).

Long-term morphodynamic modeling requires appropriate upscaling of the bed level adaptation associated with the dominant hydrodynamic processes (timescales of hours to days) to the time periods relevant for morphological changes (years to decades). Various techniques exist to accelerate bed level evolution in the model simulations, while accounting for this short-term hydrodynamic variability. These techniques range from postponed morphological updating, based on gradients in the tide-averaged residual transport, to constructing simplified sediment balances that express bottom change in terms of sediment transport gradients depending only on the local water depth (De Vriend et al., 1993; Latteux, 1995; Roelvink, 2006; Roelvink & Reniers, 2011). The most commonly used morphological updating technique is the fully coupled approach (Roelvink, 2006), where the bed level is updated every hydrodynamic time step. Such continuous updating includes short-term interactions between flow, sediment transport, and morphology, resulting in a stable bed evolution, also in intertidal areas which are inundated during high water conditions only. From a physical point of view, the hydrodynamics should be resolved as detailed as possible. For reasons of computational efficiency, long-term morphodynamic evolution is often modeled with the additional use of a so-called morphological timescale factor (or MorFac, MF), essentially a multiplication factor for the depth change (Roelvink & Reniers, 2011). Multiplication of the bed level change with MF at each computational time step leads to a reduction in computational time equal to MF. This accelerated approach resolves morphodynamic processes operating at intratidal timescales, while maintaining the speed, stability, and accuracy of tidally averaged updating approaches (Van der Wegen et al., 2008). A prerequisite for stability is that the bed level changes are small compared to water depth, so that no irreversible changes develop within a phase of the tidal cycle (Van der Wegen & Roelvink, 2008).

The upscaling of the hydrodynamic conditions (with MF) implies that the hydrodynamic period should be sufficiently short to ensure that the sequence of hydrodynamic conditions also governs the morphodynamic development (for instance, upscaling a spring-neap cycle with MF = 50 implies that spring tide occurs 1 year after neap tide) in the model. The time series of boundary conditions therefore need to be represented by a reduced number of hydrodynamic conditions consisting of a repetitive pattern that includes the dominant forcing conditions (but excludes stochastic events such as storms that strongly impact the bed evolution). The goal of input reduction is therefore to derive a representative subset of forcing conditions that is sufficiently short to be used for morphodynamic upscaling while approaching the residual transport and associated morphological changes resulting from a simulation forced with the full time series over the period of interest (i.e., a "brute-force" simulation).

Existing methods for tidal input reduction aim at capturing the dominant tidal dynamics in a single tide (e.g., Dastgheib et al., 2008; Van Maanen et al., 2013) or with two representative tidal cycles (e.g., Latteux, 1995; Lesser, 2009). Such simplified tidal signals have been shown to phenomenologically reproduce observed morphological changes of tidal channels (Dastgheib et al., 2008; Dissanayake et al., 2009; Van der Wegen & Roelvink, 2012; Van Der Wegen et al., 2011). However, strongly simplified tidal signals insufficiently capture tidal extremes (the tidal elevation above Mean High Water and below Mean Low Water) because they neglect these variations. The range of tidal water level variations influences the development of the intertidal areas. The intertidal areas, in turn, influence tidal dynamics in the channels (Friedrichs & Aubrey, 1988) and therefore simplified tidal boundary conditions influence the development of tidal asymmetry. Although a semidiurnal tide with its overtides may approximate the tide-averaged residual noncohesive bedload transport in the main estuarine channels (Van de Kreeke & Robaczewska, 1993), the long-term morphodynamic development of tidal basins is much more subtle and driven by tidal asymmetries resulting from the combination of multiple tidal constituents (Guo et al., 2016). Therefore, preserving asymmetries present in the original observed tidal signal, as well as providing the hydrodynamic conditions necessary for the development of intertidal areas, is considered a key requirement for the tidal input reduction approach. Despite its importance for long-term morphodynamic modeling, the impact of tidal input reduction methods has rarely been systematically investigated.

A systematic investigation of tidal input reduction techniques preferably correlates such techniques to morphological output. However, such a comparison is not straightforward. First, morphodynamic models are sensitive to parameterizations (e.g., the sediment transport formula) and settings (grid size and bed slope effect) used in the morphodynamic model (Baar et al., 2019; Van Maanen et al., 2011). Second, morphodynamic simulations are the result of various feedback mechanisms, diffusing the effect of the boundary schematization. In this paper, we

therefore refrain from morphodynamic simulations and focus on the effect of the tidal input reduction approach on the simulated hydrodynamic and sediment transport parameters relevant for morphodynamics.

The aim of this paper is twofold. First, a tidal input reduction technique is introduced that yields a synthetic, periodic spring-neap tidal signal representing the tidal extremes as well as tidal asymmetry. Second, the effects of both existing and the new tidal input reduction approaches are systematically investigated, since such an evaluation is missing in the literature. Simulations forced with the original tidal signal (as a reference) and simulations forced with schematized tides are evaluated in terms of tidal asymmetry, bed shear stress, inundation of intertidal flats, and residual sand transports. For this latter purpose, we develop and apply a morphostatic (i.e., no bed level updating) model of the Ems estuary (The Netherlands).

The structure of the remainder of this paper is as follows. We first review existing tidal input reduction techniques and explain the new methodology (Section 2). We then develop a numerical model of a real-world estuary (The Ems estuary, Section 3) and apply this to examine the effect of various types of tidal input reduction techniques on simulated hydrodynamics and sand transport (Section 4). The implications of simplifying tidal signals are discussed in Section 5, and conclusions are drawn in Section 6.

2. Tidal Input Reduction

2.1. The Morphological Tide

The goal of tidal input reduction is to create simplified representative tidal boundary conditions for upscaling bed level changes in process-based morphodynamic models. The aim is to represent the original tidal series in a simplified signal in a sense that it produces the same residual transport or initial morphological change patterns for a defined period and region of interest. The simplified tide is constructed as a periodic signal, so that a sequence of the same synthetic tidal signals is continuous. Such a simplified tide is often referred to as the "morphological tide" (Latteux, 1995).

The most common method to derive a morphological tide can be summarized as follows (Roelvink & Reniers, 2011). The morphological development over a sufficiently long time period (e.g., several spring-neap cycles) is executed with both full hydrodynamic forcing and with several accelerated simulations, each forced with a single tidal cycle, selected from the time series. The simulated patterns of residual transport or bed level adaptations resulting from reduced input simulations and from the full forcing simulations are subsequently compared based on a correlation coefficient and the slope of the regression. The tidal cycle that produces simulated results that best resemble the results from a full forcing simulation is then considered to be most representative.

Lesser (2009) demonstrated that such a simplified tide fails to correctly represent residual transport in some cases because it neglects the asymmetry resulting from interaction between the main semidiurnal constituent (M_2) and the main diurnal constituents (O_1 and K_1). Hoitink et al. (2003) demonstrated that in diurnal or mixed mainly diurnal regimes a residual transport can develop resulting from the tidal asymmetry that arises from these primary constituents because they have angular frequencies that consist of sums and differences of two of the basic astronomical frequencies (see Pugh, 1987), leading to substantial residual transport and morphological changes (Van Maren & Gerritsen, 2012; Van Maren et al., 2004). In these regimes, the residual transport that arises from the triad interaction of K_1, O_1, and M_2 can be more important than the residual transport caused by the nonlinear interaction of the main semidiurnal component (M_2) with its first overtide (M_4) (Song et al., 2011), often considered to be the dominant mechanism for shallow water tides (e.g., Friedrichs & Aubrey, 1988; Van de Kreeke & Robaczewska, 1993). Lesser (2009) therefore included this triad interaction by defining an artificial constituent C_1 with half the frequency of the M_2 tidal constituent. The resulting *double tide* consists of C_1, M_2, and its overtides and may include an additional scaling factor for the amplitude of M_2 and/or C_1 to account for the presence of a residual flow.

A literature review on publications that apply fully coupled accelerated process-based morphodynamic models in tide-dominated settings was performed to provide an overview of current tidal forcing approaches (Table 1). The 40 publications reviewed reveal that tidal forcing is often reduced to the M_2 tidal constituent (17 publications). All of these studies comprise idealized model configurations. In modeling studies that give a representation of a real-world estuarine environment, the tide is usually represented by M_2 and its overtides (4 publications), the empirically derived morphological tide (2 publications), or the morphological *double tide* (4 publications). These

Table 1
Tidal Forcing Approaches Used in Online-Updated Accelerated Morphodynamic Simulations

Tidal forcing	Literature
M_2	Bolla Pittaluga et al. (2015), Braat et al. (2017), Elmilady et al. (2022), Elmilady et al. (2020), Geleynse et al. (2011), Guo et al. (2015), Hibma et al. (2003), Leonardi et al. (2013), Marciano et al. (2005), Nahon et al. (2012), Van der Wegen et al. (2010), Van der Wegen and Roelvink (2008), Van der Wegen et al. (2008), Van Maanen et al. (2013), Xie et al. (2017), Yu et al. (2014), and Zhou et al. (2014)
$M_2 + M_2$ overtides	Dissanayake et al. (2009), Dastgheib et al. (2008), Nnafie et al. (2018), and Nnafie et al. (2019)
Morphological tide	Chen et al. (2022) and He et al. (2022)
Morphological double tide	Elmilady et al. (2019), Van Der Wegen et al. (2011), Van der Wegen and Roelvink (2012), and Van der Wegen and Jaffe (2014)
Full tidal forcing	Dam et al. (2008), Dam et al. (2016), Ganju and Schoellhamer (2010), Ganju et al. (2011), Ganju et al. (2009), George et al. (2012), Luan et al. (2017), Styles et al. (2016), Van der Wegen and Jaffe (2013), Van der Wegen et al. (2017), Weisscher et al. (2022), Zhang and Mao (2015), and Zheng et al. (2021)

studies aim at capturing the dominant tidal forces in a single or double representative tidal cycle. However, the (1D) simulated long-term morphodynamic development of estuarine environments is governed by the combined effects of asymmetries resulting from the interaction of multiple tidal constituents and river-tide interaction (Guo et al., 2016). Particularly, the omission of the S_2 constituent reduces the effects of river-tide interaction and tidal asymmetry, leading to an underestimation of tide-induced residual transport. Yet, the effects of ignoring significant constituents in simplified tides are not well studied for 2D morphodynamics. Presumably because of the unknown effects of oversimplifying tides in 2D morphodynamic simulations, the authors of 13 publications chose to overcome the considerations for tidal input reduction by forcing the full tide (Table 1). However, forcing accelerated morphodynamic simulations with a noncyclic tidal signal is not preferred. Incomplete tidal cycles in a representative signal have an unknown, erroneous contribution to the residual transport patterns. The unwanted effect of incomplete tidal cycles within the reduced tidal period, which are to be upscaled, can affect the subtle effects of tidal asymmetry that are the cause of residual transport in real-world conditions where tidal cycles are always completed. Although it is unknown under which conditions the error caused by incomplete tidal cycles is significant in the sediment balance for simulations of many tidal periods, a simplified cyclic tide that represents all significant tidal constituents (and therefore their interactions) would be an important advance over earlier simplified tides. The interaction between each significant tidal constituent plays a role in driving tidal residual transport and therefore in morphodynamic development (Guo et al., 2016).

2.2. A Synthetic Representative Signal

We aim to develop a generic method to construct a representative tidal signal that incorporates tidal extremes in a synthetic spring-neap cycle, while remaining periodic. The target synthetic spring-neap cycle (a) sufficiently represents the original signal to preserve asymmetries; (b) is periodic, to ensure consistency in the start and end of consecutive cycles and to control the relative phasing with other types of forcings (e.g., wind, waves, river discharge, and ecology); and (c) is derived directly from the boundary information to avoid the empirical procedure required for the *morphological tide*, which introduces a dependency on the parameters and the locations chosen for the analysis. The aim for the procedure is to provide a synthetic signal that resembles the original tidal signal, excluding variations resulting from nontidal processes.

The construction of the synthetic signal starts with a fortnightly modulation of the amplitude of the semidiurnal tide to represent spring-neap variations. A synthetic signal with the duration of a fortnight resembles more accurately the real-world amplitude and phase variation than a single or double tide. Higher harmonics of the semidiurnal tide are included to represent the asymmetry of the tide. Diurnal tides are included, following the method of Lesser (2009) to account for the O_1-K_1-M_2 interaction while maintaining periodicity of the signal. The synthetic signal is given by the following equation:

$$\begin{aligned}\zeta(t) = &\left(\overline{A_{D_2}} + A_{D_{sn}}\cos(\omega_{sn}t)\right)\cos\left(\omega_{D_2}t - \phi_{D_2}\right)\\ &+\overline{A_{D_4}}\cos\left(\omega_{D_4}t - \phi_{D_4}\right)\\ &+\overline{A_{D_6}}\cos\left(\omega_{D_6}t - \phi_{D_6}\right)\\ &+\overline{A_{D_8}}\cos\left(\omega_{D_8}t - \phi_{D_8}\right)\\ &+\overline{A_{C_1}}\cos\left(\omega_{C_1}t - \phi_{C_1}\right)\end{aligned} \quad (1)$$

where $A_{D,n}$ is the amplitude, $\omega_{D,n}$ is the angular frequency, and $\phi_{D,n}$ is the phase of the nth tidal constituent. The angular frequency ω_{D_2} is taken equal to ω_{M_2}, and all other angular frequencies are an integer product or one over an integer product of this primary forcing frequency. The diurnal C_1 constituent has an amplitude of $\sqrt{2A_{O_1}A_{K_1}}$ and the phase average of ϕ_{O_1} and ϕ_{K_1}. The overbar denotes time-averaging and t is time. The amplitude of D_{sn} modulates $\overline{A_{D_2}}$ and is equal to the amplitude of the second largest peak in the semidiurnal frequency band, which corresponds to S_2 or N_2. The length of the "morphological spring-neap cycle" we introduce is given by the closest even number of D_2 cycles that fit into the length of the spring-neap period induced by M_2-S_2 interaction; exactly 28 semidiurnal cycles. The angular frequency of the fortnightly modulation is then given by the following equation:

$$\omega_{sn} = \frac{2\pi}{28T_{D_2}} \quad (2)$$

where T_{D_2} is the period of the D_2 constituent.

The stepwise construction of the morphological spring-neap cycle is illustrated in Figure 1, using a 19-year record of water level observations collected in the Dutch North Sea (monitoring station Wierumergronden). The synthetic signal is compared with the full tidal signal using histograms of the free surface elevation (ζ) and its time derivative ($d\zeta/dt$). The histogram of ζ indicates asymmetry in tidal peaks, that is, tidal peak asymmetry, and the histogram of $d\zeta/dt$ indicates asymmetry in the duration of the rising and falling limbs of the surface elevation time series. The latter is also referred to as tidal duration asymmetry and is highly relevant for the direction and magnitude of residual bed-load transport of noncohesive sediment (Van de Kreeke & Robaczewska, 1993). This approach based on histograms concisely characterizes tidal asymmetry resulting from the interaction of all constituents, in contrast to the harmonic method that characterizes the asymmetry resulting from two or more interacting constituents. The histograms in Figure 1 illustrate how the addition of the individual terms of Equation 1 provide a signal that progressively better resembles the nearly complete tidal signal (reconstructed with 68 significant constituents resolved through harmonic analysis, see Pawlowicz et al. (2002)).

Applying basic trigonometry, the synthetic signal is rewritten as a linear combination of sines and cosines with zero phases, which facilitates the optimization. This equation is fitted to the full astronomical tidal signal using scale factors to the amplitudes of the sines and cosines of D_2, D_{sn}, C_1, and D_4 (higher harmonics of D_2 are not scaled because of time efficiency in the algorithm). A combined Root-Mean-Squared-Error (RMSE) for the histogram of ζ and $d\zeta/dt$ is computed for each individual scaling factor. The error values are stored in a matrix to optimize the combination of scaling factors for the amplitudes of each tidal constituent. The procedure described to construct the synthetic spring-neap tidal cycle is written in MATLAB code and made available for download in a toolbox called morfacTide (Schrijvershof, 2022).

Histograms of (a) the observed water levels at monitoring station Wierumergronden, (b) water levels from a full tidal reconstruction, and (c) water levels from the synthetic spring-neap cycle and other simplified tidal signals are shown in Figure 2. Representing the full tide with a single M_2 constituent clearly oversimplifies the signal as this M_2 tide is completely symmetric. Although this is slightly improved by adding an M_4 constituent, tidal extremes are not yet captured. These extremes are better represented when spring-neap variations ($M_2 + M_4 + S_2 + MS_4$) are included, but the asymmetry of ζ is reversed. The morphological *double tide* represents the asymmetry of $d\zeta/dt$ well, but does not capture the extremes and asymmetry of ζ. The synthetic spring-neap cycle better approximates the extremes and asymmetries in the full tidal signal than the other simplified tides do. The synthetic signal does include, however, a third peak in the histogram of $d\zeta/dt$, which is not present in the full tide. Apparently, this peak is suppressed by tidal constituents other than included in the simplified tide.

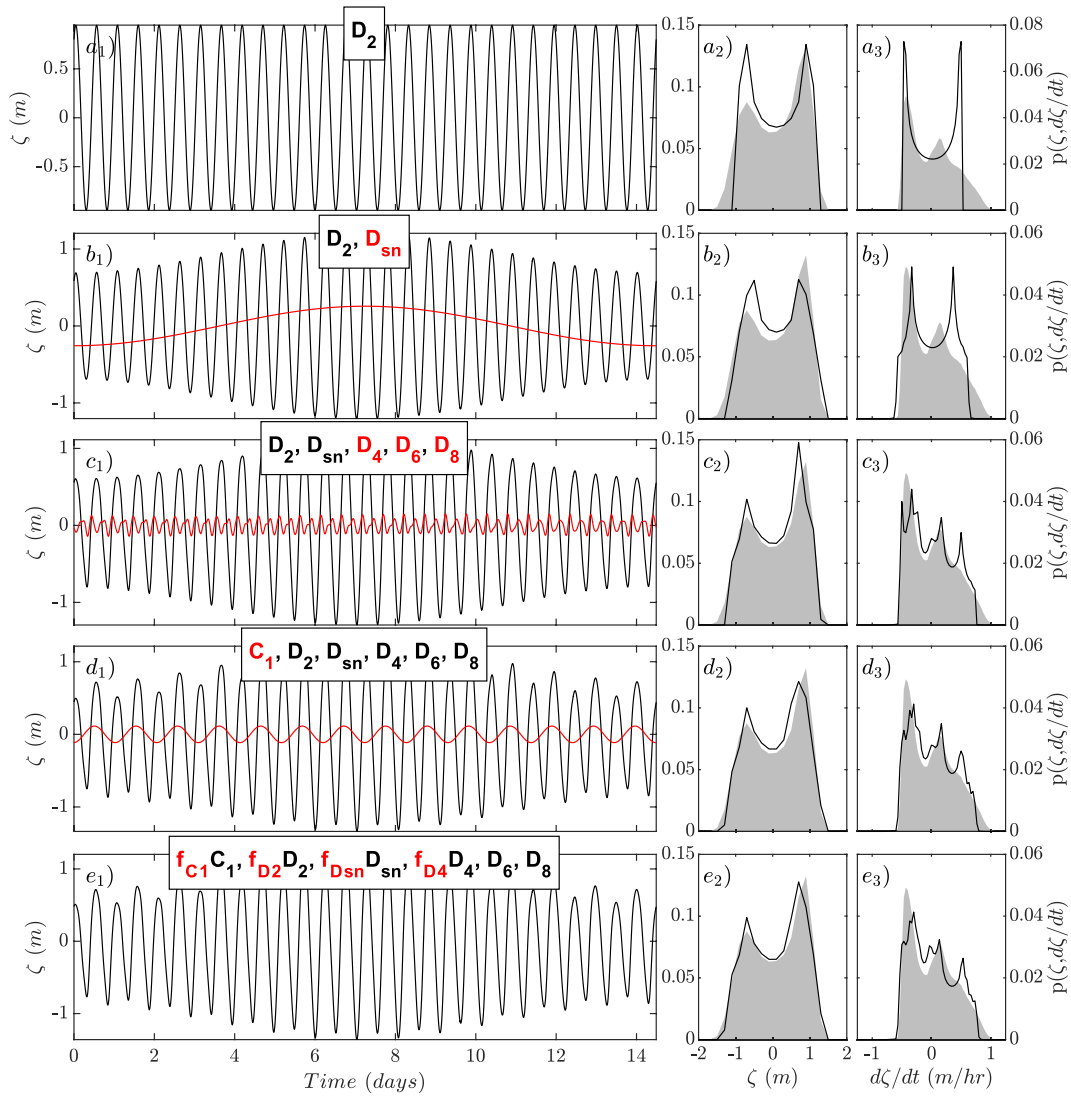

Figure 1. Step-wise construction of the synthetic spring-neap cycle, adding constituents in panel (a–d) and scaling in panel (e). For each step the resulting time series (subscripted by 1) are shown in black and the added tidal constituent in red. The panels subscripted by 2 and 3 show the histograms of the synthetic signal (continuous line) and the full tidal signal (gray patch) for ζ and $d\zeta/dt$, respectively.

3. Numerical Model

3.1. Model Set-Up

A numerical model is developed to quantify how various tidal reduction techniques influence the spatial variation of hydrodynamics and sediment transport. The model is set up to represent a real-world estuary rather than an idealized case, because the complex topography of a real environment introduces tidal asymmetries to be represented appropriately. For this purpose we have selected the Ems estuary, a meso-tidal system on the Dutch-German border that is part the Wadden Sea. The tidal prism is predominantly accommodated by a single channel that aligns with the incoming tidal wave propagation direction, as the tidal wave travels from west to east along the North Sea coast. The discharge of the main river draining into the estuary (the Ems river) varies between 30 and 300 m^3/s and is small compared to the flood tidal prism (10^9 m^3) (De Jonge et al., 2014). Other rivers discharging in the Ems estuary have a mean annual discharge that is smaller than 10 m^3/s.

The model is developed in the Delft3D Flexible Mesh model suite (Kernkamp et al., 2011). The numerical domain covers the offshore coastal part in the Wadden Sea, the estuary, and the river up to an up-estuary weir, with a

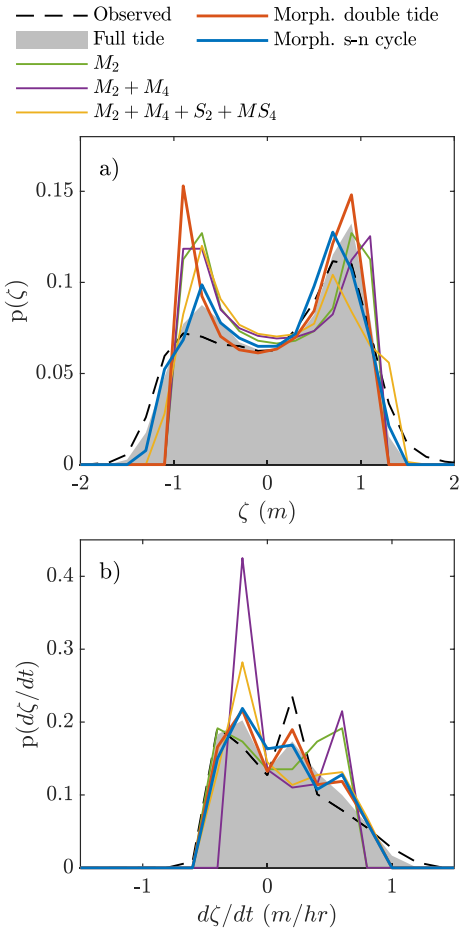

Figure 2. Histograms of (a) ζ and (b) $d\zeta/dt$ for the observed signal (dashed line), a tidal prediction including 68 resolvable tidal constituents (gray patch), and the simplified tidal signals (colored) previously used for long-term morphodynamic modeling. Histograms are constructed using a bin width of 0.2 m and $\frac{1}{6}$ m/hr for the histogram of ζ and $d\zeta/dt$, respectively.

grid cell size ranging from 1 km (offshore) to 30 m (Figure 3). The model is set-up in 2D depth-averaged (2Dh) mode, with corrections for spiral motion (secondary flow) applied to the depth-averaged momentum equations. Water level boundary conditions are derived from a validated hydrodynamic model that covers the Northwest European Shelf (Zijl & Groenenboom, 2019) for the years 2018–2019. Tidal constituents at the boundaries are adjusted according a comparison between modeled and observed amplitudes and phases, derived through harmonic analysis (Pawlowicz et al., 2002) at station Wierumergronden (close to the western boundary of the model—see Figure 3). A time-varying observed river discharge is prescribed at the upstream end of the Ems river for model calibration and validation, whereas a constant value (80 for the Ems river and less than 10 m^3/s) for the smaller rivers) is prescribed for various scenario simulations. The bathymetry of the model is based on echosounding observations collected in 2014, which are made freely available by the Dutch Directorate-General for Public Works and Water Management (https://www.rijkswaterstaat.nl/formulieren/contactformulier-servicedesk-data).

Sediment transport is computed with the Van Rijn (1993) formula for medium fine sand (180 μm). The model is executed in morphostatic mode (i.e., no bed update) because the feedback loops initiated by bed level adaptation complicates the analysis on the direct effects of the boundary schematization on hydrodynamics and residual transport. An equilibrium sand concentration is prescribed at the marine model boundaries but no sand enters the model domain through the fluvial boundaries. There is interaction with the bed, which has an unlimited sand supply potential. The simulated sediment transports in the model can deviate significantly from the natural conditions. However, the settings for the sand transport model have a limited effect on the results because the simulations are used for a relative comparison between simulations with various boundary conditions.

3.2. Hydrodynamic Calibration and Validation

Water level observations for the years 2018–2019 collected throughout the estuary are used to calibrate and validate the model (see Figure 3). The time series are decomposed into tidal constituent amplitudes and phases using harmonic analysis (Pawlowicz et al., 2002). In the calibration phase, the model simulates the year 2018, using a spatially uniform roughness coefficient, Mannings' n, amounting to 0.017, 0.019, and 0.021 $m^{1/3}\ s^{-1}$ (Figure 4). Tidal propagation is best represented by a Manning's n value of 0.019 $m^{1/3}\ s^{-1}$. Such a bed roughness, however, overestimates dampening of the tide in the Ems river. In reality, the tides amplify as a result of extensive fluid mud deposits in the Ems river, resulting in an apparent bed roughness around 0.10 $m^{1/3}\ s^{-1}$ (Van Maren, Winterwerp, & Vroom, 2015). A linear decrease in bed roughness (from 0.019 at the entrance of the river toward 0.011 $m^{1/3}\ s^{-1}$ at the upstream end at the weir) is therefore employed, which better represents the tidal dynamics.

The model was validated against water level observations over the first five months of 2019. The modeled amplitudes of the four primary tidal constituents (M_2, S_2, O_1, and K_1) and M_4 are typically within 15% of the observed amplitudes (Figure 5a). The errors are larger (up to 28%) for the S_2 and M_4 tidal constituents in the landward part of the Ems river (Figure 5b). Modeled phases are typically within 10° of observations (Figure 5c), but the modeled phases of O_1 and especially K_1 differ more than 20° in the tidal river part (Figure 5d).

The calibrated model introduced herein serves to evaluate alternative tidal input reduction approaches for morphodynamic modeling. The nonschematized tidal boundary conditions (*full tidal*, providing a reference condition) and alternative simplified tidal representations (as in Figure 2) are detailed in Table 2. The boundary forcing with the morphological *double tide* includes an analytically derived scaling factor for M_2 (see Lesser (2009) for the derivation) to incorporate the total energy of the full tide (the sum of squares of the amplitudes of all tidal constituents) in the semidiurnal frequency band. Applying the scaling factor, residual transports resulting from

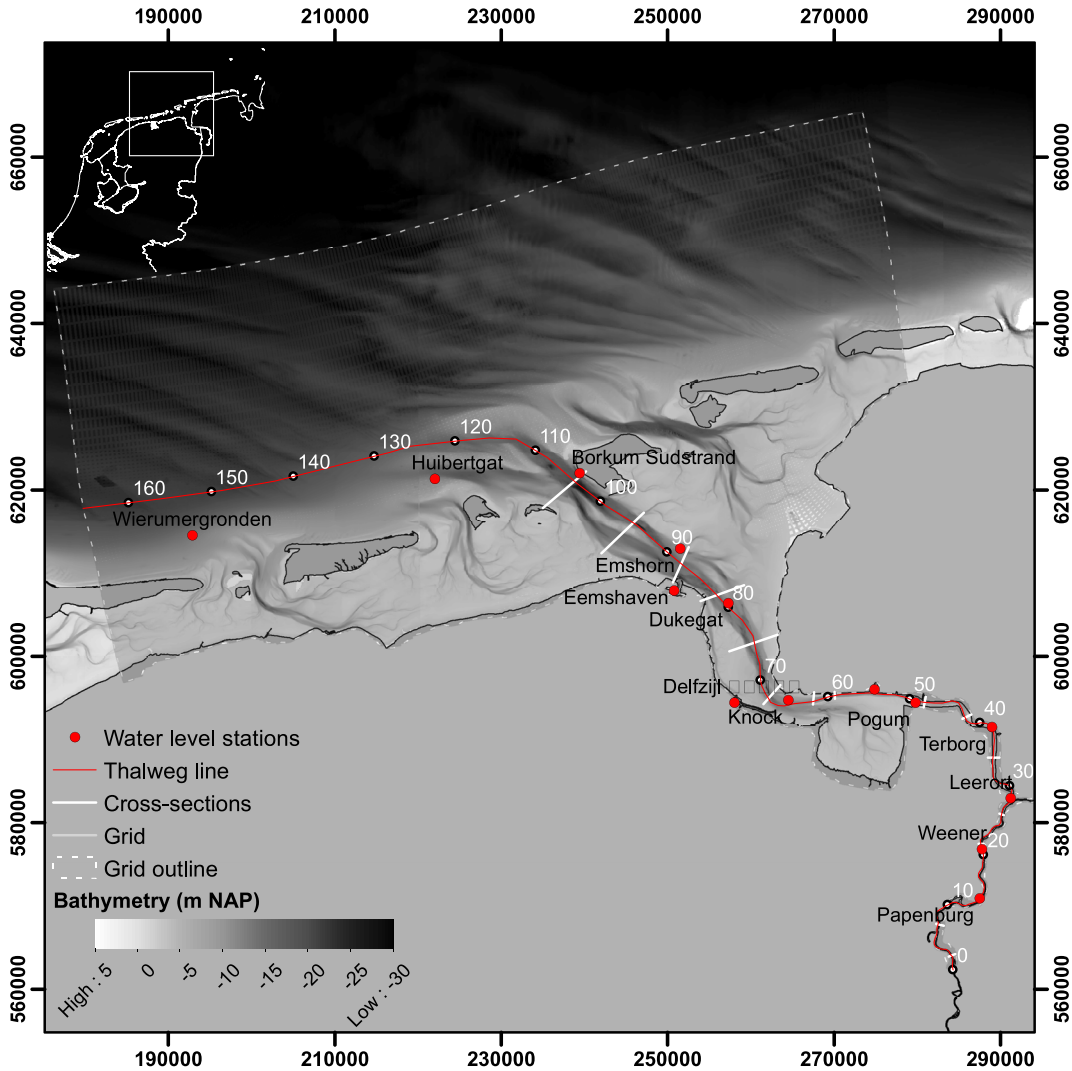

Figure 3. The Ems estuary and numerical model domain (gray lines), with the locations of water level observations (red dots) and a line that follows the main route of tidal propagation (red line) from the western boundary of the model through the thalweg of the estuary and river, with estuary kilometers defined with respect to the point of maximal tidal intrusion at the weir.

a mean (residual) flow is conserved in the simplified tide. All simulations (Table 2) are preceded by a 2-week period that is excluded from the analysis to arrive at equilibrium conditions for the hydrodynamics and suspended sediment concentrations at the start of the analysis. The next sections compare the various tidal input reduction scenarios to the reference simulation in terms of tidal wave shape, bed shear stress, inundation, and sand transport. The hydrodynamically verified *full tidal* simulation is regarded in this comparison as the best representation of reality for tidal dynamics on the scale of this particular estuary as a whole. Therefore, the tidal input reduction scenario that yields outcomes that most closely approximate those of the *full tidal* simulation is regarded as the best input reduction approach for tidal dynamics. Residual sand transports generated by the *full tidal* simulation are, however, not evaluated against observations and should not be interpreted as an attempt to calculate the fluxes of residual sediment in the real world. Many variables outside the scope of the current model setup, such as fine sediment dynamics (Van de Kreeke et al., 1997; Winterwerp, 2011), anthropogenic activity (van Maren, van Kessel, et al., 2015; Van Maren et al., 2016), and nontidal processes (Ridderinkhof et al., 2000), affect residual sediment transport in the Ems estuary. The obtained residual transport is primarily a result of the simulated tidal hydrodynamics because of the sediment model's simplified setup. The most effective input reduction approach for sediment transport is selected based on the degree in which residual transport in an alternative tidal reduction

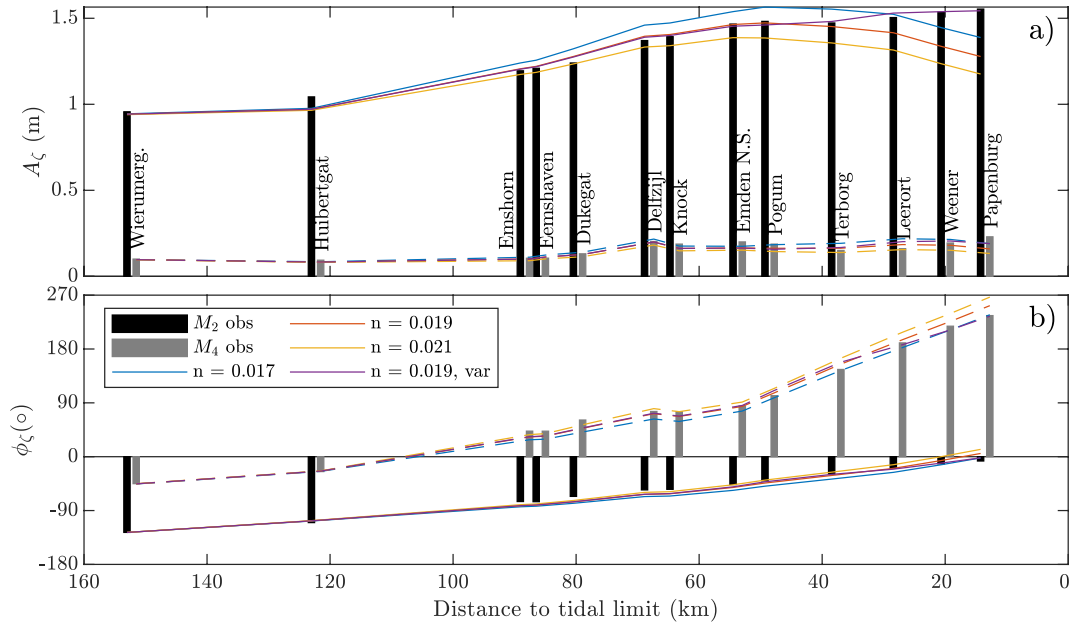

Figure 4. Observed and modeled (a) amplitudes and (b) phases of the M_2 and M_4 tidal constituents, based on the 2018 simulation. Model results (colored lines) show the effect of different values for a spatially uniform Mannings' n ($m^{1/3}$ s^{-1}) and the best calibrated model with a spatially varying roughness in the Ems river.

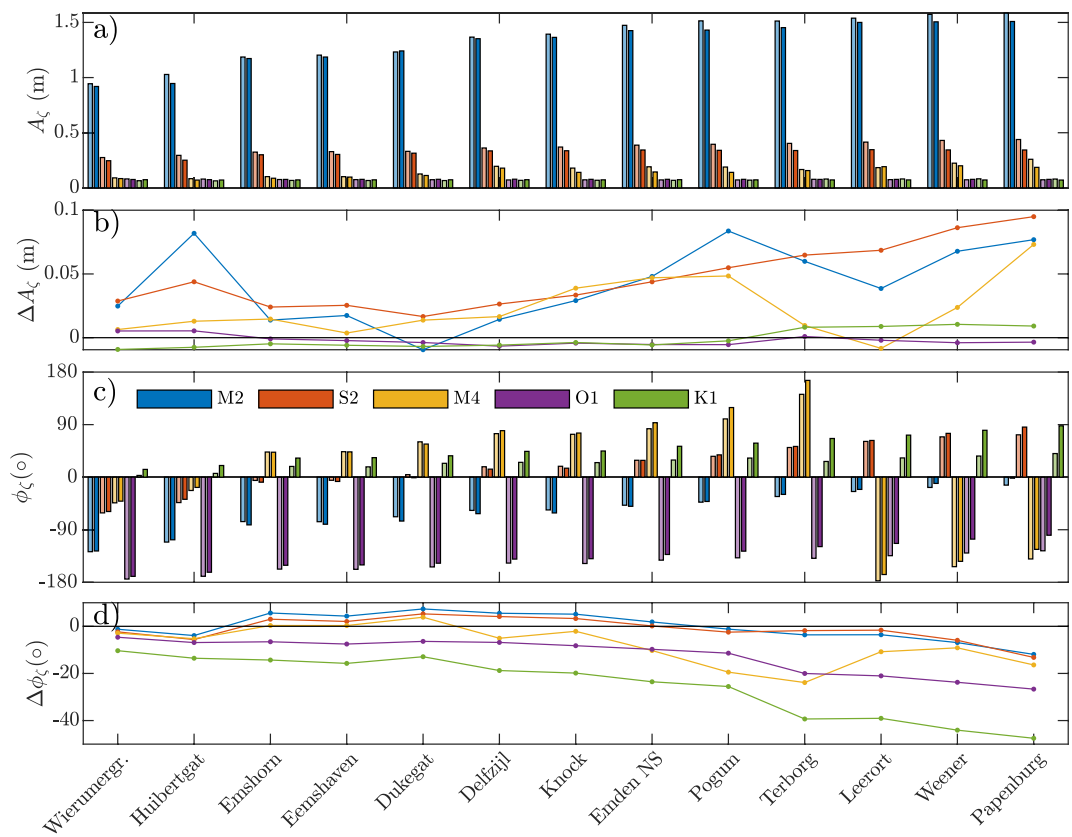

Figure 5. Observed (light colored bars) and modeled (dark colored bars) tidal constituent (a) amplitudes and (c) phases, based on the 2019 simulation. The difference (observed − modeled) of the amplitudes and phases are shown in panels (b and d), respectively.

Table 2
Duration of the Simulations Forced With Simplified Tidal Signals and the Full Tidal Simulation That Serves as the Reference

Simulation name	Duration
Full tidal	1 year
M_2	24 hr, 50 min
M_2M_4	24 hr, 50 min
$M_2M_4S_2MS_4$	14.77 days
Morphological double tide	24 hr, 50 min
Morphological spring-neap	14.48 days

Note. Simulation names are used in the legends of the figures in the results.

approach mimics the *full tidal* residual transport. This strategy is frequently applied in the setup of morphodynamic models (Roelvink & Reniers, 2011).

4. Results

4.1. Tidal Wave Shape

The representation of tidal wave shape is a primary indicator for the error made in the simulations forced with simplified tidal conditions. Figure 6 quantifies the adequacy of the tidal wave shape representation based on the RMSE between the tidal reduction scenario and the *full tidal* signal, for histograms of both ζ and $d\zeta/dt$. The figure clearly shows that only using an M_2 boundary forcing leads to the largest error. Including more tidal constituents in the boundary information decreases the error and introducing spring-neap variations ($M_2M_4S_2MS_4$) leads to a markedly better representation of tidal wave shape. The *morphological spring-neap tide* shows the smallest error, both for ζ and for $d\zeta/dt$. The improvement established by introducing spring-neap variations is largest in the coastal and central parts of the estuary (70–160 km) because error estimates for all tidal reduction techniques converge to the same value in the upper reaches of the estuary.

4.2. Bed Shear Stress

The estuary's thalweg maximum bed shear stress magnitudes are most properly represented when spring-neap variations are taken into consideration (Figure 7a, Table 2). The tidal wave shape is better retained and therefore asymmetries are better preserved leading to higher maximum tidal velocities. Despite accounting for spring-neap variations, the maximum bed shear stress is still underpredicted by 30%–40% because the *Full tidal* simulation includes maxima that happen when several tidal constituents amplify each other, and not all of these constituents are represented in the synthetic spring-neap cycle. The estuary thalweg's mean bed shear stresses (Figure 7b), on the other hand, are represented well by all simplified tides (although they are slightly overpredicted using the morphological *double tide*.). Maximum shear stresses are largest in the main tidal channels (Figure 8a) and, consequently, absolute improvements are largest in the tidal channels when accounting for spring-neap variations (compare in Figures 8d and 8f to Figures 8b, 8c, and 8e). However, maximum shear stresses on the intertidal areas are also underpredicted, in all simulated scenarios. A quantification of the error made in representing bed shear stress magnitudes over the complete model domain (presented in Figure 8) indicates that both the maximum (Figure 9a) and the mean (Figure 9b) shear stress magnitudes improve by incorporating tidal extremes. A reduction in RMSE is found in the subtidal (channels) and intertidal parts of the model domain. The consistent overprediction of mean bed shear stress magnitudes with the morphological *double tide* in the thalweg (Figure 7b) is reflected by larger RMSE values in the subtidal domain (Figure 9b). Possibly, the overprediction is due to the implementation of a scaling factor for the M_2 tidal amplitude to account for nontidal energy in the spectral tidal frequency band.

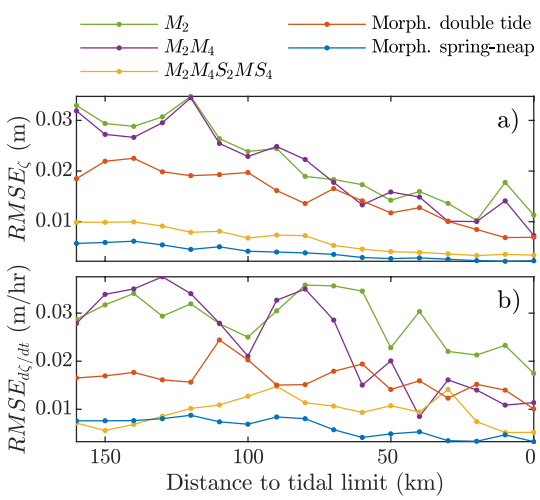

Figure 6. Root-Mean-Squared-Error for the histogram of (a) ζ and (b) $d\zeta/dt$ between the simulations forced with simplified tides and the *full tidal* simulation, calculated at points in the thalweg along the estuary kilometers defined in Figure 3.

4.3. Inundation

The intertidal areas, represented by computational cells that experience regular flooding and drying, make up ≈ 20% of the model domain. In those areas, the duration of inundation strongly controls sediment dynamics and therefore, the residence time of water over the tidal flats (Figure 10) is an important property to capture in morphodynamic simulations of tidal environments with tidal flats. Particularly the high littoral zone (Figures 10a and 10b) is not captured by the simulations that exclude spring-neap variations, evidenced by too many computational cells that are permanently dry. Sediment cannot settle or erode in the higher intertidal parts when those areas never inundate. The bed level height of tidal flats will not be able to adjust to a height that

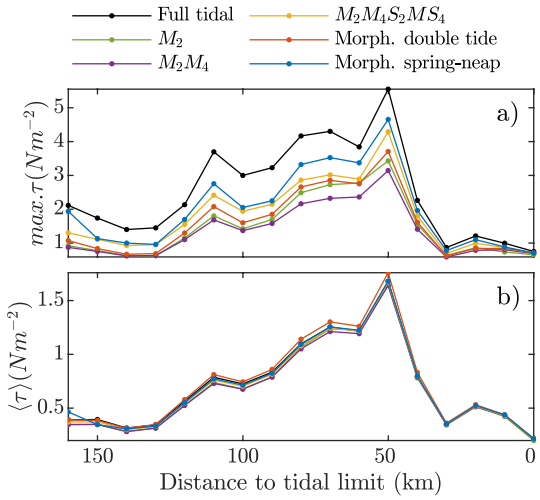

Figure 7. (a) Maximum and (b) mean bed shear stress magnitudes simulated with the *full tidal* forcing and simplified tides, calculated at points in the thalweg along the estuary kilometers defined in Figure 3.

resembles reality. Similarly, in the low littoral zone (Figures 10e and 10f), the simplified signals without spring-neap variations result in too many computational cells that are permanently inundated such that the lower intertidal zone becomes a subtidal area. Average conditions in the midlittoral zone are well-represented by all simplified tides.

4.4. Sediment Transport

The gross, cross-section integrated sand transport fluxes vary with each tidal cycle in the *full tidal* simulation. The mean of the range in gross transport flood fluxes (Figure 11a) is well-captured by the $M_2M_4S_2MS_4$ tide, the *morphological double tide*, and the *morphological spring-neap* simulations. The M_2 tide, the *morphological double tide*, and the *morphological spring-neap* simulations all reproduce the mean gross ebb transports reasonably well. For the *full tidal* simulation, the residual transport (Figure 11b) is flood-dominant at the mouth (85–108 km), ebb-dominant in the central part (45–85 km) of the estuary, and neither flood nor ebb dominant in the tidal river (0–45 km). This large-scale behavior is captured well by each of the alternative simplified tides, except for the M_2 simulation, which prescribes a perfectly symmetric tide at the sea boundaries and therefore leads to an underestimation of the flood directed residual transport (Figure 11a). The *morphological spring-neap* tidal boundary conditions lead to residual transport best representing *full tidal* residual transport (Figure 11b). The M_2M_4 and $M_2M_4S_2MS_4$ tidal boundary conditions lead to an underestimation of the magnitude of the residual transport fluxes, and the *morphological double tide* generates slightly more ebb-dominant transport in the entire estuary.

The representation of the *full tidal* residual sand transport magnitudes and directions at each individual computational cell (Figure 12) indicates a general pattern in the results. The M_2 simulation does not capture the residual sand transport accurately. The M_2M_4 and *morphological double tide* represent the patterns in the channels fairly well (Figure 12d) and, to some degree, this also holds for the magnitudes in the lower littoral zone (Figure 12c1).

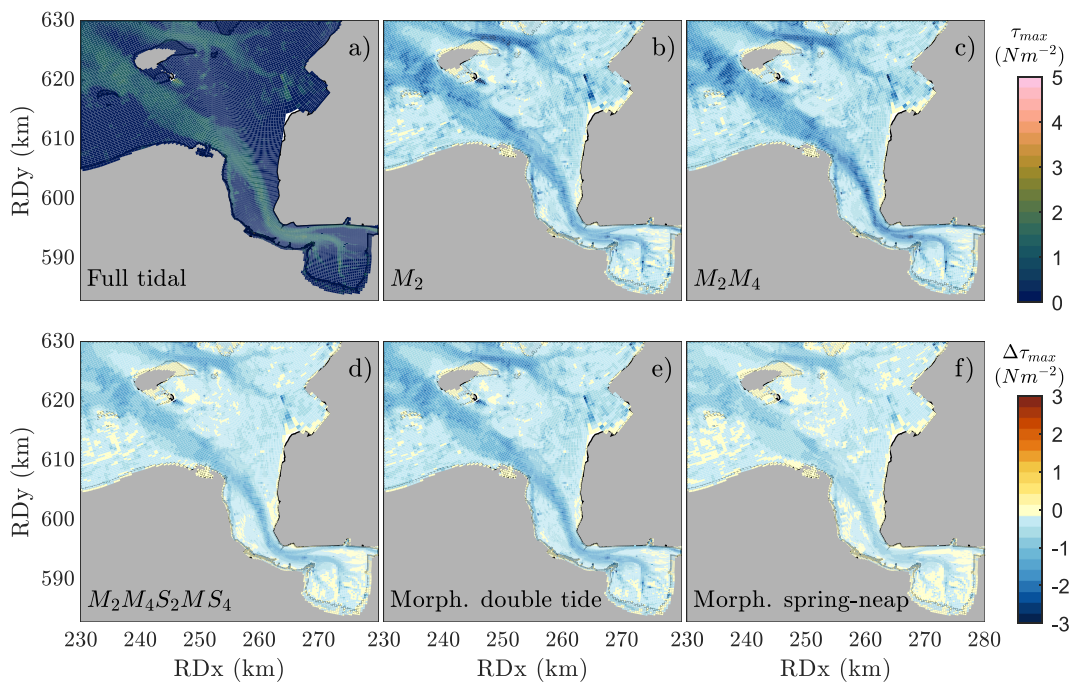

Figure 8. Maximum bed shear stress magnitude during the reference simulation (a) and difference in maximum bed shear stress magnitude between the scenarios and the reference (b–f).

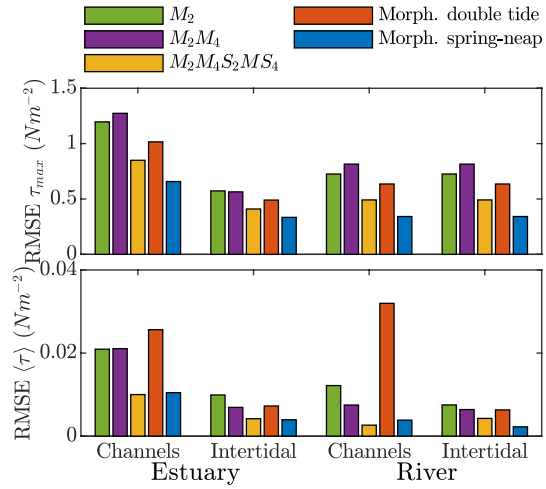

Figure 9. Root-Mean-Squared-Error (RMSE) for the (a) maximum and (b) mean bed shear stress magnitudes between the simulations forced with simplified tides and the *full tidal* simulation. RMSE values are calculated as mean values for all the computational cells within the specified subregions estuary, river, subtidal channels, and intertidal areas.

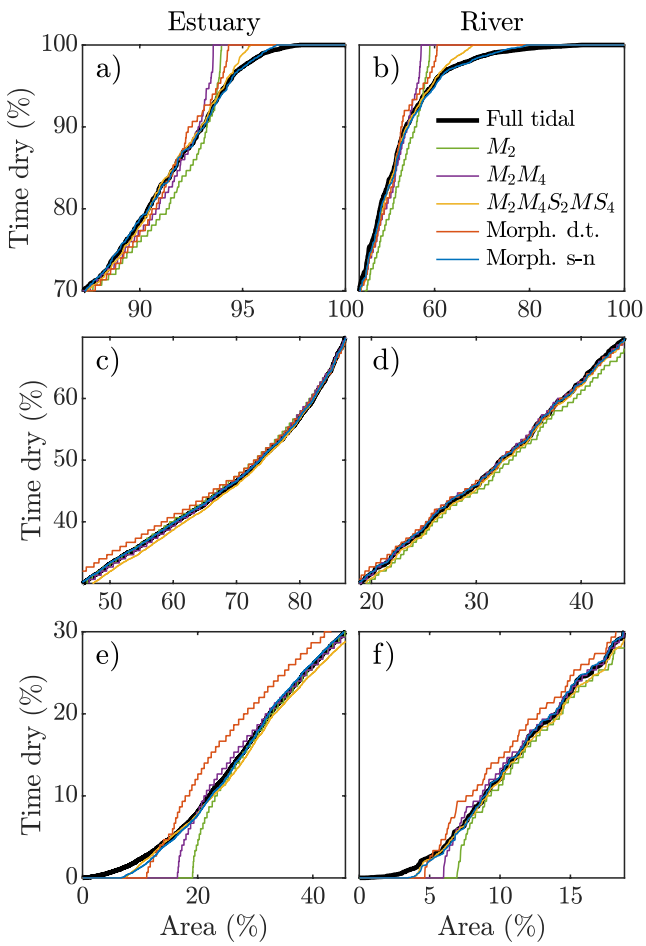

Figure 10. Cumulative distributions of the fraction of time of the total simulation length (in %) that a computational cell is dry (emerged), as a function of the fraction of the total intertidal area in the modeling domain. The distributions are shown for defined subregions; (a, c, and e) the estuary and (b, d, and f) the river, and subdivided in the (a and b) high, (c and d) mid, and (e and f) lower littoral zone.

However, inclusion of spring-neap variations is required for a more accurate representation of sand transport magnitudes and directions in the midlittoral and higher littoral zone (Figures 12a and 12b). Summarizing this information, an analysis on the error (RMSE) made in the direction and magnitude of residual transports averaged over all computational cells (Figure 13) reveals that particularly the error in direction is smaller for the simulations that include spring-neap variations. The RMSE for the magnitude of the residual transport shows less scatter, except for the M_2 simulations, which clearly deviates in the channels. In general, including spring-neap variations reduces the error in magnitude and direction of residual transports in the channels and over the intertidal areas.

5. Discussion

A new tidal input reduction method was developed which includes periodic spring-neap variation in a simplified tide. Prescribing this new method as boundary conditions in an estuarine setting improves the representation of tidal wave shape, maximum and mean bed shear stress magnitudes, inundation times, and residual sand transport patterns, compared to existing tidal input reduction methods to represent the nonschematized tidal dynamics. The strong and weak points of the new methodology and existing tidal input reduction techniques are summarized in Figure 14 for a number of metrics using a normalized score defined as follows:

$$score = \frac{z}{\max(z)}, z = 1 - \frac{x}{\max(x)} \quad (3)$$

The x-values are binary (metrics *Periodic* and *Deterministic*), proceed directly from Table 2 (*Cycle length*), or they are continuous (model scenario metrics from Chapter 4). The continuous x-values are computed per scenario and defined as an averaged RMSE between the output for that particular metric computed with a simplified and a full tidal signal. The most accurate scenario scores a value of 1, the least accurate scenario a value of 0. The new method scores maximal for 10 out of 12 metrics, with lower scores only for the duration of the cycle and the duration of inundation (second-best score).

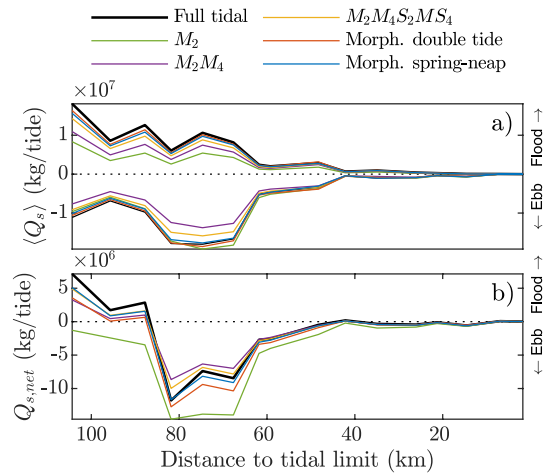

Figure 11. Mean of the total (bed + suspended) load gross transport fluxes (a) and residual transport per tidal cycle (b) in the thalweg (see the cross-sections in Figure 3 for locations).

Also, the new method scores considerably better than all other tidal input reduction techniques for metrics that determine the morphodynamic evolution of a model (bed shear stress parameters, sand transport, inundation, and tidal asymmetry). The hydrodynamic forcing of any morphodynamic model using the new tidal input reduction technique is therefore physically more realistic than conventional techniques, although at this point we do not verify our technique with morphodynamic simulations because of dependencies on parameter settings and complex morphodynamic feedbacks.

The main drawback of the synthetic spring-neap cycle, following directly from Figure 14, is the duration of the simulation. The required 28 M_2 cycles (≈14.48 days) is a 14 times longer period than that of a *morphological double tide* (Lesser, 2009). This does not lead to longer simulations, however, since shorter hydrodynamic periods (as in the conventional techniques) are simply repeated more frequently (e.g., Dastgheib et al., 2008). Single tides may only lead to faster simulations when combined with a higher value for MF, but a higher MF also amplifies errors and therefore morphologic instabilities.

Our methodology does require more careful considerations on the forcing of nontidal boundary conditions. Numerical morphological models may also be driven by nontidal processes, such as a seasonally varying river discharge (e.g., He et al., 2022; Van Der Wegen et al., 2011) or wave- and wind-driven resuspension (e.g., Van der Wegen et al., 2017). Such nontidal forcings need to be adjusted for upscaling (with annual events recurring MF times per year). For these conditions, the relative phases of the tidal and the nontidal forcing need careful examination to prevent, for instance, seasonal river flooding to persistently coincide with spring tides. But where the phase difference of successive M_2-S_2 spring-neap tidal cycles differ, they are identical for successive synthetic spring-neap cycles. This entails the risk of a more systematic correlation with nontidal forcing.

A tide-averaged transport for coarse sediment may be generated by a representative tide consisting of a tide-induced Eulerian mean current (M_0), M_2 and any of its even overtides (Van de Kreeke & Robaczewska, 1993). When diurnal components are important, a similar net residual transport arises from the triad interaction of M_2-K_1-O_1 (Hoitink et al., 2003), which can be captured in a periodic double tide through an artificial diurnal component with half the frequency of M_2 (Lesser, 2009). Spring-neap variations are so far mainly ignored in representative tides (Dastgheib et al., 2008; Roelvink & Reniers, 2011). This paper demonstrates that simplified tides consisting of a single or a double tide (which are most frequently used for long-term morphodynamic modeling) do perform well in representing mean bed shear stress and residual sand transports inside the estuarine channels. However, they fail to reproduce the full range of asymmetries in the tide, leading to an underestimation of maximum bed shear stresses (controlling the timescales of bed level adaptation) and full tidal range, which in turn controls the development of intertidal flats (Friedrichs, 2011). Our methodology also better represents residual sand transport over the intertidal flats, probably because the velocity skew (flood vs. ebb dominance) over tidal flats is modulated during the spring-neap cycle (Nidzieko & Ralston, 2012). For environments where intertidal areas are small or low-dynamic, the spring-neap variations in a representative tide may be ignored. But whenever the

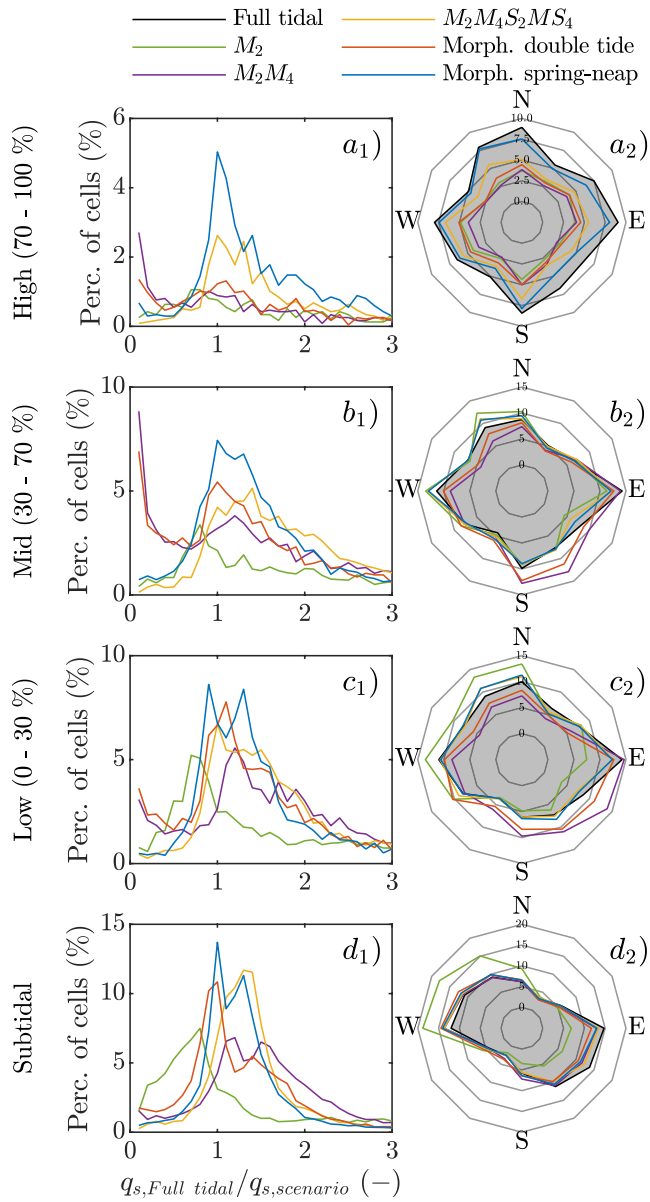

Figure 12. Histograms (in % of all computational cells) of the ratio of the time-averaged residual sand transport magnitudes in the *Full tidal* simulation and simplified tidal input reduction scenarios (left column, subscripted by 1). A value $q_{s,Fulltidal}/q_{s,scenario} < 1(>1)$ indicates that transport magnitudes in the *Full tidal* simulation are smaller (larger) (overprediction and underprediction by the scenarios, respectively). Circular representations of histograms of the time-averaged residual sand transport directions (clockwise from geographic north) for all simulations, binned by 30° classes (right column, subscripted by 2). Radial axes indicate the percentage of cells within a class. The rows in the figure (a–d) separate the distributions for the (a) high, (b) mid, and (c) low littoral zone, and (d) the subtidal part of the modeling domain.

intertidal areas in the modeling domain are important for the estuary-scale morphodynamic development, a *single* or *double tide* oversimplifies the hydrodynamic forcing.

Applying the synthetic spring-neap cycle in a fully coupled morphodynamic model (including bed level adaptations) leads to much more realistic tidal dynamics. Including the tidal extremes and asymmetries resulting from the spring-neap modulations will lead to an improved representation of the nonschematized residual sand transport, presumably promoting a more realistic channel transport and channel-shoal exchange. The inclusion of tidal extremes, however, may also have negative effects. The resulting higher maximum bed shear stresses possibly further restrict the upper limit for the morphological acceleration factor because the higher sediment

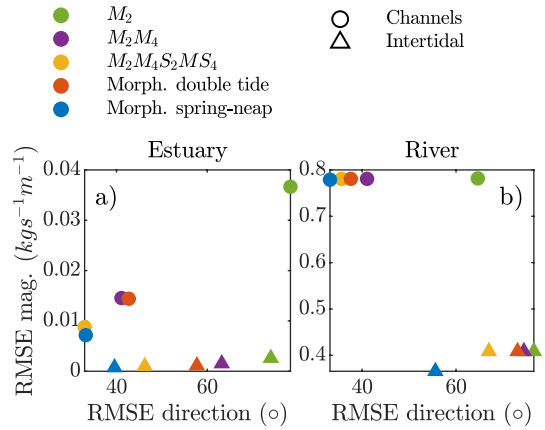

Figure 13. Error (Root Mean Square Error) in the direction (horizontal axis) and magnitude (vertical axis) of the residual total (bed + suspended) load sand transport in the channels (circles) and on the intertidal areas (triangles).

transport rates can lead to an overexaggeration of the upscaled morphological response (Ranasinghe et al., 2011). Such a potential shortcoming depends on various model settings (Reyns et al., 2014) and requires a case-specific analysis. Furthermore, the gross and net sand transport presented in this paper was computed using a single sand fraction and the Van Rijn (1993) formula. Multiple fraction sediment beds, including cohesive sediments, may develop unexpected interactions in conjunction with the synthetic spring-neap cycle which needs to be explored as part of future work. Planned long-term morphodynamic modeling will reveal the advantages and the challenges of the more realistic representation of tidal dynamics advocated in this paper.

6. Conclusions

Spring-neap variations can be included in simplified tidal signals as boundary conditions in long-term morphodynamic models. Compared to a single or a double tide, often used in morphodynamic simulations, the tidal variation in a synthetic spring-neap cycle is more realistically represented through a fortnightly modulation of the amplitude of the semidiurnal tide. The tidal input reduction method developed in this paper yields a signal that (a) resembles the amplitude variation of the full tidal signal and sufficiently preserves asymmetries to approach nonschematized tidal dynamics and residual sand transports; (b) is strictly periodic; and (c) can readily be derived from the original tidal signal or harmonic constituents. It does not require a fitting procedure based on modeling results.

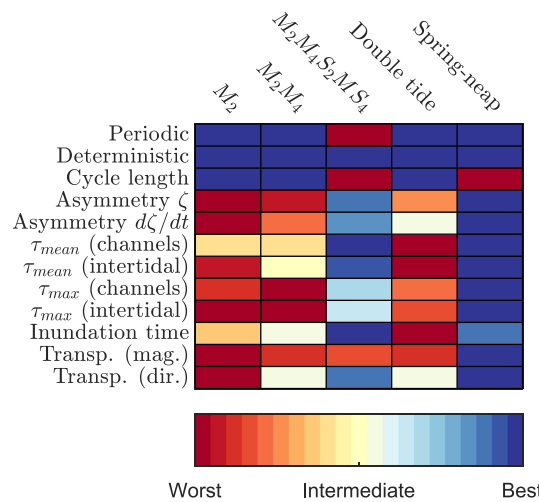

Figure 14. Normalized scores (0–1) for simplified tides to represent (simulated) nonschematized tidal conditions. The calculation of the score values is explained in the main text.

When the tidal extremes caused by spring-neap variation are included in the boundary conditions, the shape of the tidal wave through the tidal basin is more realistically reproduced, which is demonstrated using a process-based numerical model of a meso-tidal estuary with multiple channels and tidal flats. Simulations with simplified tidal signals that neglect the tidal extremes underestimate maximum bed shear stresses in the channels and simulate a too limited extent of the tidal flats. Although simulations forced with these simplified signals approximate the tidally averaged residual sand transport patterns in the channels simulated with nonschematized tidal series, an appropriate representation of the extremes is required to reproduce the magnitudes and directions both in the channels and on the intertidal areas. Hence, the newly developed tidal input reduction method provides a signal that resolves the simulated full tidal noncohesive residual sediment transport within the estuary more accurately compared to the existing tidal input reduction approaches used in the past.

Data Availability Statement

A toolbox is developed that allows to construct a synthetic spring-neap tidal cycle from a time series of tidal elevations. The toolbox is developed in MATLAB code and available for download at https://github.com/Rschrijvershof/morfacTide.git (Schrijvershof, 2022). There are no restrictions on the data used in this study. The bathymetry data used for model setup was requested through the servicedesk data of Rijkswaterstaat (https://www.rijkswaterstaat.nl/formulieren/contactformulier-servicedesk-data). Observed water level data from Dutch monitoring stations are available at https://waterinfo.rws.nl and the data from the German monitoring stations were requested at WSA Ems-Norsee (https://www.wsa-ems-nordsee.wsv.de/). The numerical model simulations used in this article are performed with the Delft3D Flexible Mesh suite, release 2021.05 (https://www.deltares.nl/en/software/delft3d-flexible-mesh-suite/). The configurations for all simulations used for the article (Schrijvershof et al., 2022) are stored and available at 4TU.ResearchData (https://doi.org/10.4121/19845262.v1).

Acknowledgments
This work was funded by the Netherlands Organisation for Scientific Research (NWO) within Vici project "Deltas out of shape: regime changes of sediment dynamics in tide-influenced deltas" (Grant NWO-TTW 17062) and Deltares Research Funds. The data presented in this paper stem from the Dutch Rijkswaterstaat, the German Wasserstrassen-und Schifffartsamt (WSA) Ems-Nordsee, and the Niedersächsischer Landesbetrieb für Wasserwirtschaft, Küsten-und Naturschutz (NLWKN). The modeling software Delft3D Flexible Mesh was made available by Deltares via the Delft3D Educational Service Package.

References

Baar, A. W., Boechat Albernaz, M., van Dijk, W. M., & Kleinhans, M. G. (2019). Critical dependence of morphodynamic models of fluvial and tidal systems on empirical downslope sediment transport. *Nature Communications*, *10*(1), 4903. https://doi.org/10.1038/s41467-019-12753-x

Bolla Pittaluga, M., Tambroni, N., Canestrelli, A., Slingerland, R., Lanzoni, S., & Seminara, G. (2015). Where river and tide meet: The morphodynamic equilibrium of alluvial estuaries. *Journal of Geophysical Research: Earth Surface*, *120*(1), 75–94. https://doi.org/10.1002/2014JF003233

Braat, L., Van Kessel, T., Leuven, J. R., & Kleinhans, M. G. (2017). Effects of mud supply on large-scale estuary morphology and development over centuries to millennia. *Earth Surface Dynamics*, *5*(4), 617–652. https://doi.org/10.5194/esurf-5-617-2017

Chen, K., He, Z., Liu, J., Lin, Y., & Jia, L. (2022). Long-term morphological evolution and its mechanism of Lingdingyang Estuary: Interferences from anthropogenic forcings. *Marine Geology*, *450*, 106856. https://doi.org/10.1016/j.margeo.2022.106856

Dam, G., Bliek, A. J., Labeur, R. J., Ides, S. J., & Plancke, Y. M. (2008). Long term process-based morphological model of the Western Scheldt Estuary. In C. M. Dohmen-Janssen & S. J. M. H. Hulscher (Eds.), (Eds). *Proceedings of 5th IAHR symposium of the River, Coastal and Estuarine Morphodynamics Conference*, (Vol. 2, pp. 1077–1084). https://doi.org/10.1201/noe0415453639-c135

Dam, G., Van Der Wegen, M., Labeur, R. J., & Roelvink, D. (2016). Modeling centuries of estuarine morphodynamics in the Western Scheldt Estuary. *Geophysical Research Letters*, *43*(8), 3839–3847. https://doi.org/10.1002/2015GL066725

Dastgheib, A., Roelvink, J. A., & Wang, Z. B. (2008). Long-term process-based morphological modeling of the marsdiep tidal basin. *Marine Geology*, *256*(1–4), 90–100. https://doi.org/10.1016/j.margeo.2008.10.003

De Jonge, V. N., Schuttelaars, H. M., van Beusekom, J. E., Talke, S. A., & de Swart, H. E. (2014). The influence of channel deepening on estuarine turbidity levels and dynamics, as exemplified by the Ems estuary. *Estuarine, Coastal and Shelf Science*, *139*, 46–59. https://doi.org/10.1016/j.ecss.2013.12.030

De Swart, H. E., & Zimmerman, J. T. (2009). Morphodynamics of tidal inlet systems. *Annual Review of Fluid Mechanics*, *41*(1), 203–229. https://doi.org/10.1146/annurev.fluid.010908.165159

De Vriend, H. J., Zyserman, J., Nicholson, J., Roelvink, J. A., Péchon, P., & Southgate, H. N. (1993). Medium-term 2DH coastal area modelling. *Coastal Engineering*, *21*(1–3), 193–224. https://doi.org/10.1016/0378-3839(93)90050-I

Dissanayake, D., Roelvink, J. A., & Van der Wegen, M. (2009). Modelled channel patterns in a schematized tidal inlet. *Coastal Engineering*, *56*(11–12), 1069–1083. https://doi.org/10.1016/j.coastaleng.2009.08.008

Elmilady, H., van der Wegen, M., Roelvink, D., & Jaffe, B. E. (2019). Intertidal area disappears under sea level rise: 250 Years of morphodynamic modeling in San Pablo Bay, California. *Journal of Geophysical Research: Earth Surface*, *124*(1), 38–59. https://doi.org/10.1029/2018JF004857

Elmilady, H., Van Der Wegen, M., Roelvink, D., & van der Spek, A. (2020). Morphodynamic evolution of a fringing Sandy shoal: From tidal levees to sea level rise (pp. 1–21). https://doi.org/10.1029/2019JF005397

Elmilady, H., van der Wegen, M., Roelvink, D., & van der Spek, A. (2022). Modeling the morphodynamic response of estuarine intertidal shoals to sea-level rise. *Journal of Geophysical Research: Earth Surface*, *127*(1), 1–26. https://doi.org/10.1029/2021JF006152

Friedrichs, C. T. (2011). *Tidal flat morphodynamics: A synthesis* (Vol. 3). Elsevier Inc. https://doi.org/10.1016/B978-0-12-374711-2.00307-7

Friedrichs, C. T., & Aubrey, D. G. (1988). Nonlinear tidal distortion in shallow well-mixed estuaries. *Estuarine, Coastal and Shelf Science*, *30*(3), 321–322. https://doi.org/10.1016/0272-7714(90)90054-U

Ganju, N. K., Jaffe, B. E., & Schoellhamer, D. H. (2011). Discontinuous hindcast simulations of estuarine bathymetric change: A case study from Suisun Bay, California. *Estuarine, Coastal and Shelf Science*, *93*(2), 142–150. https://doi.org/10.1016/j.ecss.2011.04.004

Ganju, N. K., & Schoellhamer, D. H. (2010). Decadal-timescale estuarine geomorphic change under future scenarios of climate and sediment supply. *Estuaries and Coasts*, *33*(1), 15–29. https://doi.org/10.1007/s12237-009-9244-y

Ganju, N. K., Schoellhamer, D. H., & Jaffe, B. E. (2009). Hindcasting of decadal-timescale estuarine bathymetric change with a tidal-timescale model. *Journal of Geophysical Research*, *114*(4), F04019. https://doi.org/10.1029/2008JF001191

Geleynse, N., Storms, J. E., Walstra, D. J. R., Jagers, H. R., Wang, Z. B., & Stive, M. J. (2011). Controls on river delta formation; insights from numerical modelling. *Earth and Planetary Science Letters*, *302*(1–2), 217–226. https://doi.org/10.1016/j.epsl.2010.12.013

George, D. A., Gelfenbaum, G., & Stevens, A. W. (2012). Modeling the hydrodynamic and morphologic response of an estuary restoration. *Estuaries and Coasts*, *35*(6), 1510–1529. https://doi.org/10.1007/s12237-012-9541-8

Guo, L., van der Wegen, M., Roelvink, D., & He, Q. (2015). Exploration of the impact of seasonal river discharge variations on long-term estuarine morphodynamic behavior. *Coastal Engineering*, *95*, 105–116. https://doi.org/10.1016/j.coastaleng.2014.10.006

Guo, L., Wegen, M. V. D., Wang, Z. B., Roelvink, D., & He, Q. (2016). Exploring the impacts of multiple tidal constituents and varying river flow on long-term, large-scale estuarine morphodynamics by means of a 1-D model. *Journal of Geophysical Research: Earth Surface*, *121*(5), 1000–1022. https://doi.org/10.1002/2016JF003821

He, Z., Liang, M., Jia, L., Dong, H., Chen, K., Liu, J., et al. (2022). Long-term morphological modeling and implication for estuarine regulation of the modaomen estuary, pearl river delta, China. *Applied Ocean Research*, *123*, 103184. https://doi.org/10.1016/j.apor.2022.103184

Hibma, A., de Vriend, H., & Stive, M. (2003). Numerical modelling of shoal pattern formation in well-mixed elongated estuaries. *Estuarine, Coastal and Shelf Science*, *57*(5–6), 981–991. https://doi.org/10.1016/S0272-7714(03)00004-0

Hoitink, A. J., Hoekstra, P., & Van Maren, D. S. (2003). Flow asymmetry associated with astronomical tides: Implications for the residual transport of sediment. *Journal of Geophysical Research*, *108*(10), 1–8. https://doi.org/10.1029/2002jc001539

Hoitink, A. J., Nittrouer, J. A., Passalacqua, P., Shaw, J. B., Langendoen, E. J., Huismans, Y., & van Maren, D. S. (2020). Resilience of river deltas in the anthropocene. *Journal of Geophysical Research: Earth Surface*, *125*(3), 1–24. https://doi.org/10.1029/2019JF005201

Kernkamp, H. W. J., Van Dam, A., Stelling, G. S., & De Goede, E. D. (2011). Efficient scheme for the shallow water equations on unstructured grids with application to the continental shelf. *Ocean Dynamics*, *61*(8), 1175–1188. https://doi.org/10.1007/s10236-011-0423-6

Latteux, B. (1995). Techniques for long-term morphological simulation under tidal action. *Marine Geology*, *126*(1–4), 129–141. https://doi.org/10.1016/0025-3227(95)00069-B

Leonardi, N., Canestrelli, A., Sun, T., & Fagherazzi, S. (2013). Effect of tides on mouth bar morphology and hydrodynamics. *Journal of Geophysical Research: Oceans*, *118*(9), 4169–4183. https://doi.org/10.1002/jgrc.20302

Lesser, G. (2009). An approach to medium-term coastal morphological modelling. Retrieved from http://www.narcis.nl/publication/RecordID/oai:tudelft.nl:uuid:62caa573-4fc0-428e-8768-0aa47ab612a9

Luan, H. L., Ding, P. X., Wang, Z. B., & Ge, J. Z. (2017). Process-based morphodynamic modeling of the Yangtze Estuary at a decadal timescale: Controls on estuarine evolution and future trends. *Geomorphology*, *290*, 347–364. https://doi.org/10.1016/j.geomorph.2017.04.016

Marciano, R., Wang, Z. B., Hibma, A., De Vriend, H. J., & Defina, A. (2005). Modeling of channel patterns in short tidal basins. *Journal of Geophysical Research*, *110*(1), 1–13. https://doi.org/10.1029/2003JF000092

Nahon, A., Bertin, X., Fortunato, A. B., & Oliveira, A. (2012). Process-based 2DH morphodynamic modeling of tidal inlets: A comparison with empirical classifications and theories. *Marine Geology*, *291–294*, 1–11. https://doi.org/10.1016/j.margeo.2011.10.001

Nidzieko, N. J., & Ralston, D. K. (2012). Tidal asymmetry and velocity skew over tidal flats and shallow channels within a macrotidal river delta. *Journal of Geophysical Research*, *117*(3), 1–17. https://doi.org/10.1029/2011JC007384

Nnafie, A., de Swart, H. E., De Maerschalck, B., Van Oyen, T., van der Vegt, M., & van der Wegen, M. (2019). Closure of secondary basins causes channel deepening in estuaries with moderate to high friction. *Geophysical Research Letters*, *46*(22), 13209–13216. https://doi.org/10.1029/2019GL084444

Nnafie, A., Van Oyen, T., De Maerschalck, B., van der Vegt, M., & van der Wegen, M. (2018). Estuarine Channel evolution in response to closure of secondary basins: An observational and morphodynamic modeling study of the Western Scheldt Estuary. *Journal of Geophysical Research: Earth Surface*, *123*(1), 167–186. https://doi.org/10.1002/2017JF004364

Pawlowicz, R., Beardsley, B., & Lentz, S. (2002). Classical tidal harmonic analysis including error estimates in MATLAB using T_TIDE. *Computers & Geosciences*, *28*(8), 929–937. https://doi.org/10.1016/S0098-3004(02)00013-4

Pugh, D. T. (1987). *Tides, surges and mean sea level*. John Wiley and Sons Ltd. Retrieved from https://www.osti.gov/biblio/5061261

Ranasinghe, R., Swinkels, C., Luijendijk, A., Roelvink, D., Bosboom, J., Stive, M., & Walstra, D. J. (2011). Morphodynamic upscaling with the MORFAC approach: Dependencies and sensitivities. *Coastal Engineering*, *58*(8), 806–811. https://doi.org/10.1016/j.coastaleng.2011.03.010

Reyns, J., Dastgheib, A., Ranasinghe, R., Luijendijk, A., Walstra, D.-J., & Roelvink, D. (2014). Morphodynamic upscaling with the morfac approach in tidal conditions: The critical morfac. *Coastal Engineering Proceedings*, *1*(34), 27. https://doi.org/10.9753/icce.v34.sediment.27

Ridderinkhof, H., Van der Ham, R., & Van der Lee, W. (2000). Temporal variations in concentration and transport of suspended sediments in a channel-flat system in the Ems-Dollard estuary. *Continental Shelf Research*, *20*(12–13), 1479–1493. https://doi.org/10.1016/S0278-4343(00)00033-9

Roelvink, D. (2006). Coastal morphodynamic evolution techniques. *Coastal Engineering*, *53*(2–3), 277–287. https://doi.org/10.1016/j.coastaleng.2005.10.015

Roelvink, D., & Reniers, A. (2011). *A guide to modeling coastal morphology* (Advances i ed.). WORLD SCIENTIFIC. https://doi.org/10.1142/7712

Schrijvershof, R. A. (2022). morfacTide. [Software]. Retrieved from https://zenodo.org/badge/latestdoi/453933163

Schrijvershof, R. A., van Maren, D. S., Torfs, P. J. J. F., & Hoitink, A. J. F. (2022). Numerical model configurations for "A synthetic spring-neap tidal cycle for long-term morphological modelling". [Dataset]. https://doi.org/10.4121/19845262.v1

Song, D., Wang, X. H., Kiss, A. E., & Bao, X. (2011). The contribution to tidal asymmetry by different combinations of tidal constituents. *Journal of Geophysical Research*, *116*(12), 1–12. https://doi.org/10.1029/2011JC007270

Styles, R., Brown, M. E., Brutsché, K. E., Li, H., Beck, T. M., & Sánchez, A. (2016). Long-term morphological modeling of barrier island tidal inlets. *Journal of Marine Science and Engineering*, *4*(4), 65. https://doi.org/10.3390/jmse4040065

Syvitski, J. P., Kettner, A. J., Overeem, I., Hutton, E. W., Hannon, M. T., Brakenridge, G. R., et al. (2009). Sinking deltas due to human activities. *Nature Geoscience*, *2*(10), 681–686. https://doi.org/10.1038/ngeo629

Van de Kreeke, J., Day, C. M., & Mulder, H. P. (1997). Tidal variations in suspended sediment concentration in the Ems estuary: Origin and resulting sediment flux. *Journal of Sea Research*, *38*(1–2), 1–16. https://doi.org/10.1016/S1385-1101(97)00040-3

Van de Kreeke, J., & Robaczewska, K. (1993). Tide-induced residual transport of coarse sediment; Application to the EMS estuary. *Netherlands Journal of Sea Research*, *31*(3), 209–220. https://doi.org/10.1016/0077-7579(93)90022-K

Van der Wegen, M., Dastgheib, A., & Roelvink, J. A. (2010). Morphodynamic modeling of tidal channel evolution in comparison to empirical PA relationship. *Coastal Engineering*, *57*(9), 827–837. https://doi.org/10.1016/j.coastaleng.2010.04.003

Van der Wegen, M., & Jaffe, B. E. (2013). Towards a probabilistic assessment of process-based, morphodynamic models. *Coastal Engineering*, *75*, 52–63. https://doi.org/10.1016/j.coastaleng.2013.01.009

Van der Wegen, M., & Jaffe, B. E. (2014). Processes governing decadal-scale depositional narrowing of the major tidal channel in San Pablo Bay, California, USA. *Journal of Geophysical Research: Earth Surface*, *119*(5), 1136–1154. https://doi.org/10.1002/2013JF002824

Van Der Wegen, M., Jaffe, B. E., & Roelvink, J. A. (2011). Process-based, morphodynamic hindcast of decadal deposition patterns in San Pablo Bay, California, 1856–1887. *Journal of Geophysical Research*, *116*(2), 1–22. https://doi.org/10.1029/2009JF001614

Van der Wegen, M., & Roelvink, J. A. (2008). Long-term morphodynamic evolution of a tidal embayment using a two-dimensional, process-based model. *Journal of Geophysical Research*, *113*(3), 1–23. https://doi.org/10.1029/2006JC003983

Van der Wegen, M., & Roelvink, J. A. (2012). Reproduction of estuarine bathymetry by means of a process-based model: Western Scheldt case study, The Netherlands. *Geomorphology*, *179*, 152–167. https://doi.org/10.1016/j.geomorph.2012.08.007

Van der Wegen, M., Van der Werf, J., De Vet, L., & Robke, B. (2017). Hindcasting Westerschelde mouth morphodynamics (1963–2011). (Tech. Rep.).

Van der Wegen, M., Wang, Z., Savenije, H. H., & Roelvink, J. A. (2008). Long-term morphodynamic evolution and energy dissipation in a coastal plain, tidal embayment. *Journal of Geophysical Research*, *113*(3), 1–22. https://doi.org/10.1029/2007JF000898

Van Maanen, B., Coco, G., & Bryan, K. (2011). A numerical model to simulate the formation and subsequent evolution of tidal channel networks. *Australian Journal of Civil Engineering*, *9*(1), 61–72. https://doi.org/10.1080/14488353.2011.11463969

Van Maanen, B., Coco, G., & Bryan, K. R. (2013). Modelling the effects of tidal range and initial bathymetry on the morphological evolution of tidal embayments. *Geomorphology*, *191*, 23–34. https://doi.org/10.1016/j.geomorph.2013.02.023

Van Maren, D. S., & Gerritsen, H. (2012). Residual flow and tidal asymmetry in the Singapore Strait, with implications for resuspension and residual transport of sediment. *Journal of Geophysical Research*, *117*(4), 1–18. https://doi.org/10.1029/2011JC007615

Van Maren, D. S., Hoekstra, P., & Hoitink, A. J. (2004). Tidal flow asymmetry in the diurnal regime: Bed-load transport and morphologic changes around the Red River Delta. *Ocean Dynamics*, *54*, 424–434. https://doi.org/10.1007/s10236-003-0085-0

Van Maren, D. S., Oost, A. P., Wang, Z. B., & Vos, P. C. (2016). The effect of land reclamations and sediment extraction on the suspended sediment concentration in the Ems Estuary. *Marine Geology*, *376*, 147–157. https://doi.org/10.1016/j.margeo.2016.03.007

van Maren, D. S., van Kessel, T., Cronin, K., & Sittoni, L. (2015). The impact of channel deepening and dredging on estuarine sediment concentration. *Continental Shelf Research*, *95*, 1–14. https://doi.org/10.1016/j.csr.2014.12.010

Van Maren, D. S., Winterwerp, J. C., & Vroom, J. (2015). Fine sediment transport into the hyper-turbid lower Ems River: The role of channel deepening and sediment-induced drag reduction. *Ocean Dynamics*, *65*(4), 589–605. https://doi.org/10.1007/s10236-015-0821-2

Van Rijn, L. C. (1993). Principles of sediment transport in rivers, estuaries and coastal seas.

Weisscher, S. A., Baar, A. W., van Belzen, J., Bouma, T. J., & Kleinhans, M. G. (2022). Transitional polders along estuaries: Driving land-level rise and reducing flood propagation. *Nature-Based Solutions*, *2*, 100022. https://doi.org/10.1016/j.nbsj.2022.100022

Winterwerp, J. C. (2011). Fine sediment transport by tidal asymmetry in the high-concentrated Ems River: Indications for a regime shift in response to channel deepening. *Ocean Dynamics*, *61*(2–3), 203–215. https://doi.org/10.1007/s10236-010-0332-0

Xie, D., Gao, S., Wang, Z. B., Pan, C., Wu, X., & Wang, Q. (2017). Morphodynamic modeling of a large inside sandbar and its dextral morphology in a convergent estuary: Qiantang Estuary, China. *Journal of Geophysical Research: Earth Surface*, *122*(8), 1553–1572. https://doi.org/10.1002/2017JF004293

Yu, Q., Wang, Y., Flemming, B., & Gao, S. (2014). Scale-dependent characteristics of equilibrium morphology of tidal basins along the Dutch-German North Sea Coast. *Marine Geology*, *348*, 63–72. https://doi.org/10.1016/j.margeo.2013.12.005

Zhang, S., & Mao, X. Z. (2015). Hydrology, sediment circulation and long-term morphological changes in highly urbanized Shenzhen River estuary, China: A combined field experimental and modeling approach. *Journal of Hydrology*, *529*, 1562–1577. https://doi.org/10.1016/j.jhydrol.2015.08.027

Zheng, J., Elmilady, H., Röbke, B., Taal, M., Wang, Z., Prooijen, B., et al. (2021). The impact of wind-waves and sea level rise on the morphodynamics of a sandy estuarine shoal. *Earth Surface Processes and Landforms*, *46*(15), 1–18. https://doi.org/10.1002/esp.5207

Zhou, Z., Coco, G., Jimenez, B., Olabarrieta, M., Van der Wegen, M., & Townend, I. (2014). Morphodynamics of river-influenced back-barrier tidal basins: The role of landscape and hydrodynamic settings. *Water Resources Research*, *50*(50), 3826–3851. https://doi.org/10.1002/2014WR015891

Zijl, F., & Groenenboom, J. (2019). *Development of a sixth generation model for the NW European shelf (DCSM-FM 100m)* (Tech. Rep.). Deltares.